 

PACS numbers: 42.55.Vc; 52.50.Jm; 36.40.Wa
DOI: 10.1070/QE2013v043n12ABEH015271

# 32.8-nm X-ray laser produced in a krypton cluster jet

E.P. Ivanova, A.Yu. Vinokhodov

*Abstract.* **We have interpreted the well-known experimental quantum yield data for a 32.8-nm X-ray laser operating at the $3d^94d$ ($J = 0$)–$3d^94p$ ($J = 1$) transition of $Kr^{8+}$ with the use of gaseous krypton or a krypton cluster jet. Proceeding from our model we propose a novel scheme for the 32.8-nm laser produced in a krypton cluster jet. The quantum yield is shown to saturate for a plasma length of ~300 μm, a krypton ion density $n_{Kr} \sim (4-9)\times10^{19}$ cm$^{-3}$, and an electron temperature $T_e \sim 5000$ eV. In this case, the energy conversion coefficient amounts to $\sim5\times10^{-3}$ of the pump pulse energy. We propose the experimental setup for producing a high-efficiency subpicosecond X-ray laser in a krypton cluster jet.**

***Keywords:*** *X-ray laser simulation, multiply charged ions.*

## 1. Introduction

The past decade has seen investigations of cluster jets with high-intensity IR laser radiation aimed at production of a hot dense plasma, which is a far-UV radiation source. The production mechanism of such cluster plasmas is the optical field ionisation (OFI) of clusters in the jet. One of the lines of this research involves the development of an X-ray laser (XRL) with a radiation wavelength $\lambda = 1-40$ nm. A compact 32.8-nm XRL with a quantum yield of $10^{12}$ photons per pulse, which is suited to many applications, has been made to date [1]. The conversion coefficient achieved in Ref. [1] is equal to $5\times10^{-6}$.

The realisation of an XRL in a cluster jet is a milestone in the path to development of an XRL in solid nanostructured targets pumped by a laser of sufficiently high intensity. An obvious virtue of cluster plasmas is the relative ease of changing the plasma parameters by varying the gas pressure in the vessel connected to the nozzle. The high intensity of laser radiation implies the use of longitudinal pumping. However, as the pump beam travels through the target, this pumping is attended with an increase in radial nonuniformity of the plasma, which entails different values of the refractive index for the propagating beam in different plasma regions. Therefore, the longer the plasma column, the greater its radial nonuniformity and, consequently, the higher the output XRL radiation divergence, which is responsible for deterioration of coherence. To date it has been determined that sufficiently high coherence in the longitudinal pumping may be obtained for a target length of several millimetres. In this connection, techniques are being developed to maintain coherence by producing more uniform plasmas with the use of additional pump pulses. We believe that there is another approach: the quest for high-efficiency XRLs in an ultrashort-length plasma in which it is possible to achieve giant values of the gain owing to its sufficiently high density ($n_i \geqslant 4\times10^{19}$ cm$^{-3}$) and temperature (no less than 5 keV).

**E.P. Ivanova** Institute of Spectroscopy, Russian Academy of Sciences, ul. Fizicheskaya 5, Troitsk, 142190 Moscow, Russia;
e-mail: eivanova@isan.troitsk.ru;
**A.Yu. Vinokhodov** State Research Centre of Russian Federation 'Troitsk Institute for Innovation and Fusion Research', ul. Pushkovykh, Bldg 12, Troitsk, 142190 Moscow, Russia;
e-mail: avinikhod@triniti.ru

Received 9 July 2013; revision received 2 October 2013
*Kvantovaya Elektronika* **43** (12) 1099–1106 (2013)
Translated by E.N. Ragozin

## 2. Formulation of the problem

Lemoff et al. [2] outlined three similar XRL schemes on the $^1S_0-{}^1P_1$ transitions of rare-gas atoms: $Ar^{8+}$, $Kr^{8+}$, $Xe^{8+}$ (Fig. 1). For each of these ions it is possible to implement a three-level lasing scheme due to a strong electron collisional monopole pumping of the upper working level $^1S_0$, a fast radiative decay of the lower working level $^1P_1$, and a relatively strong radiative transition from the upper working level to the lower one. The radiative transition rates obtained in our calculations as well as the wavelengths of the principal laser transition are indicated in Fig. 1. Given in Ref. [2] are the lifetimes of the working levels $^1S_0$ and $^1P_1$, which permit calculating the radiative transition probabilities for these levels. The probabilities for the radiative decay of the $^1P_1$ level to the ground state agree nicely with the well-known results of calculations obtained under different approximations. According to our calculations, the radiative $^1S_0-{}^1P_1$ transition probabilities are equal to $4.69\times10^9$, $1.64\times10^{10}$, and $1.3\times10^{10}$ s$^{-1}$ for $Ar^{8+}$, $Kr^{8+}$, and $Xe^{8+}$, respectively. These values are substantially lower than the rates of these transitions known from the literature, which are in poor agreement with each other.

The reasons for discordance between the probabilities of this transition under different theoretical approaches are discussed in Ref. [3]. Weaker and longer-wavelength laser transitions from the upper working level $^1S_0$ are also possible to the $^3P_1$ level in $Ar^{8+}$ and to the $^3D_1$ level in $Kr^{8+}$ and $Xe^{8+}$ (these levels are indicated with dashed lines in Fig. 1). The wavelength of this transition in $Kr^{8+}$ is $\lambda = 33.5$ nm. For each of the ions, the probability of this radiative transition is approximately three times lower than the principal $^1S_0-{}^1P_1$ transition probability.

The above-threshold ionisation of an atomic system interacting with a high-intensity electromagnetic field was considered in the framework of a classical theoretical approach in Ref. [4]. The authors of Ref. [2] estimated the threshold inten-

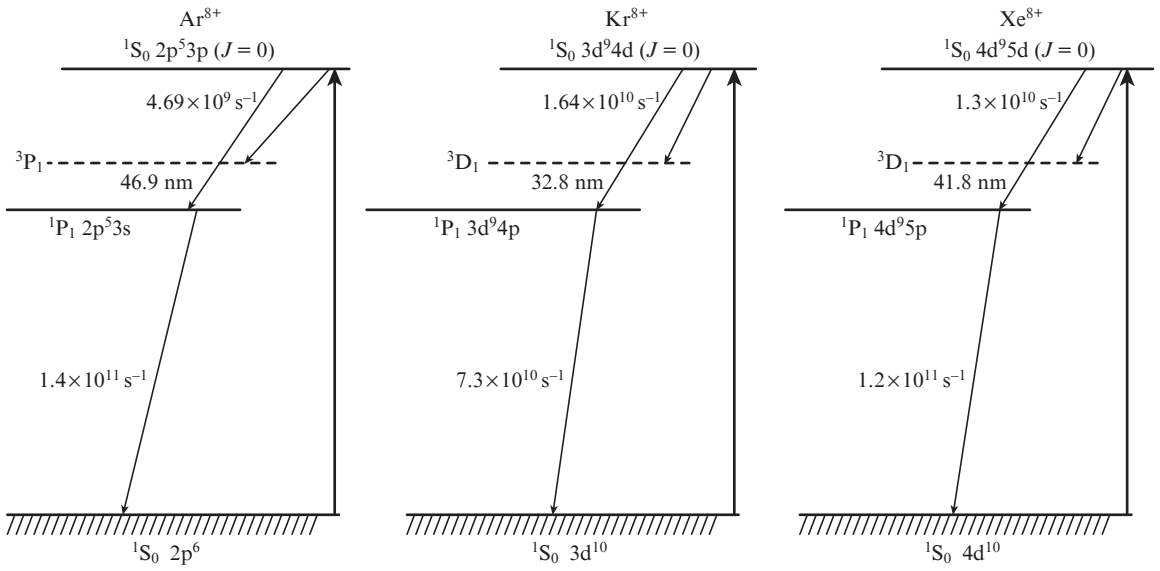


**Figure 1.** Three XRL schemes on the $^1S_0 - {}^1P_1$ transition in the rare-gas ions $Ar^{8+}$, $Kr^{8+}$, and $Xe^{8+}$.

sity of the electromagnetic field for the ionisation of eight electrons in Ar, Kr, and Xe atoms with the use of formulas from Ref. [4]. For krypton it was no less than $10^{17}$ W cm$^{-2}$; to ionise the ninth electron from the $3d^{10}$ shell in $Kr^{8+}$ requires a nine times higher intensity. For this reason we assume in this work, like in Ref. [2], that ~90% of the ions are in the $Kr^{8+}$ state immediately after the action of the femtosecond pulse. According to Refs [2, 4], the electron energy distribution at the instant of detachment of eight electrons from a krypton atom is eight δ functions with energies ranging from 12 to 1050 eV. For a $Kr^{8+}$ ion density of no less than $10^{18}$ cm$^{-3}$, the electron energy thermalisation (Maxwellisation) proceeds during a subpicosecond time interval (of the order of 100 fs for a density of no less than $10^{19}$ cm$^{-3}$).

Figure 2 shows the rates of monopole excitation by electron impact from the ground state of the working ion to the upper working state $^1S_0$. Note that the data in Fig. 2 are in good agreement with the corresponding data calculated by other authors. From Fig. 2 it follows that the rate of monopole excitation for $Ar^{8+}$ is approximately two orders of magnitude lower than for $Xe^{8+}$ and an order of magnitude lower than for $Kr^{8+}$. So low an excitation rate gives rise to a small population inversion so that the highest values of the gain $g(t)$ do not exceed 1–2 cm$^{-1}$ under optimal conditions [5, 6]. This is obviously insufficient for affording a high quantum yield for interaction lengths of about several millimetres.

The model of a high-efficiency 41.8-nm XRL in Pd-like $Xe^{8+}$ was elaborated in Ref. [7]. The plasma was assumed to result from the interaction of a xenon cluster jet with the femtosecond optical field of intensity no lower than $10^{16}$ W cm$^{-2}$. The pump conditions required for making a subpicosecond $Xe^{8+}$ XRL, also with the use of a xenon cluster jet, were determined in Ref. [8]: a quantum yield of $10^{13}$ photons per pulse is possible for a plasma of length $L = 0.3$ mm and diameter $d \sim 20$ μm for a xenon density $2.5\times10^{19}$ cm$^{-3}$.

One can see from Figs 1 and 2 that in $Kr^{8+}$ the rates of radiative transitions and those induced by collisions with electrons are approximately two times lower than for $Xe^{8+}$. About the same is also true for other transitions that determine kinetics of excited level populations in $Kr^{8+}$. We note that this is precisely the circumstance which underlies the unique possibility for making a high-efficiency $Kr^{8+}$ XRL with an ultrashort pulse duration.

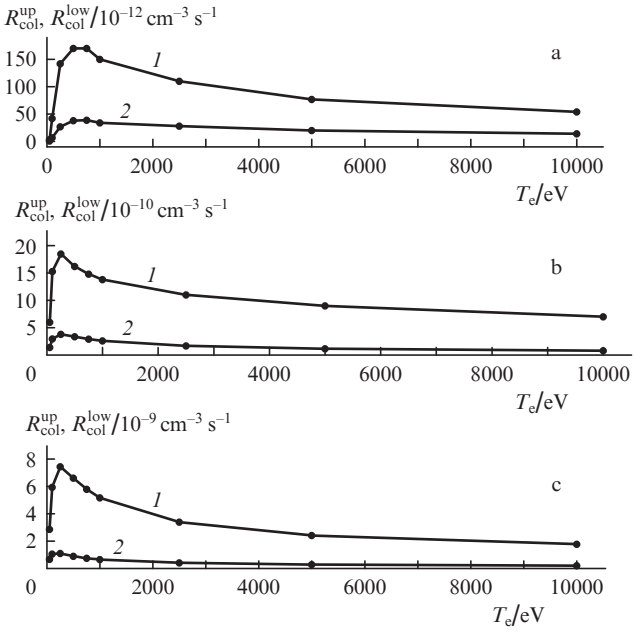


**Figure 2.** Electron collisional excitation rates for the upper [$R_{col}^{up}$; (*1*)] and lower [$R_{col}^{low}$; (*2*)] working levels in (a) $Ar^{8+}$, (b) $Kr^{8+}$, and (c) $Xe^{8+}$.

In the present work we performed atomic kinetic calculations of the emission spectra for Ni-like Kr ions. The level population kinetics includes, apart from the ground state, 54 excited energy levels of the $3d^94l$ ($l$ = s, …, f) configurations and 13 levels of the $3p^53d^{10}4s$ and $3p^53d^{10}4p$ configurations lying below the ionisation limit, i.e. 68 levels in all. The inclusion of the latter 13 highly excited levels was not of fundamental importance and was made for verifying the calculation stability against variations of the number of states included.

In our calculations we assumed that:

1. The plasma is produced in the form of a cylinder of diameter $d$ and length $L$ due to the propagation of a laser beam through a cluster jet of thickness $L$.

2. The parameters of the pump pulse are such that the plasma with an electron temperature $T_e$ is formed immediately after cessation of the optical field–cluster interaction, the $Kr^{8+}$ ions residing in the ground state and accounting for 90% of the plasma ions.

3. The electron ($T_e$) and ion ($T_i$) temperatures as well as the plasma diameter ($d$) are uniform over the volume and invariable throughout the XRL operation time.

4. The electron and ion energy distributions are Maxwellian; in this case, the form of the distribution is of no great significance to the calculations of transition rates induced by electron–ion collisions.

5. The ion temperature in the cluster plasma $T_i = T_e$. In the plasma produced by the OFI technique in krypton, $T_i = T_e/4$.

We do not calculate the amplification dynamics for the spontaneous emission propagating through the plasma; one of the possible approaches to such a calculation involves solution of the Maxwell–Bloch equations [9, 10]. These calculations are required for determining the saturation of the gain $g(t)$ with plasma length $L$. In the case under consideration (like in the overwhelming majority of experiments) the gain is observed in the regime of working ion ionisation to higher ionisation stages. The working ion lifetime determines, in principle, the length $L$. In Ref. [11] it is proposed to use the estimate $gL \sim 14–15$, whereby saturation with length sets in. We employ a similar approach to determine the saturation length; however, in our work the $gL$ product is much greater.

In our calculation the gain $g(t)$ was averaged over the spatial and time coordinates. To this end, the cylinder target was divided into layers of length shorter than the 'length' of the pump pulse; the elementary processes in each layer will then take proceed in a similar way, but with a time delay. In this case, it suffices to average the $g(t)$ function only over time. The theoretical model was considered in our earlier works (see papers [6–8] as well as references therein).

Section 3 is concerned with interpretation of the results of experimental observation of spontaneous emission amplification on the $\lambda = 32.8$ nm transition in $Kr^{8+}$ in the plasma produced in the interaction of gaseous krypton with the optical pump field [12–14]. Interpreted in Section 4 are the experimental data of Refs [15, 16], where the active medium was produced in the interaction of a krypton cluster jet with the pump field. Calculations performed in the framework of the model of a high-efficiency ultrashort-pulse XRL at $\lambda = 32.8$ nm are outlined in Section 5, and the experimental facility required for the implementation of this model is discussed in Section 6.

## 3. Interpretation of experimental results on the observation of X-ray lasing in gaseous krypton

The gains $g(t)$ in the Ni-like krypton ions $Kr^{8+}$ were first calculated by the authors of Ref. [12], who emphasised a strong dependence of these coefficients on the temperature $T_e$. An experimental measurement of the gain $g$ was made in Ref. [13], in which the plasma with the population inversion was produced under longitudinal laser pumping of gaseous krypton confined in a cell. The quantum yield of the 32.8-nm XRL output as a function of cell length was recorded with a CCD. The pumping was effected by the circularly polarised 30-fs radiation pulses of a Ti:sapphire laser with a pulse energy of 760 mJ. The radiation was focused to a spot several millimetres distant from the input to the krypton-filled cell. The actual working diameter $d$ was not determined in Ref [13]. According to our estimates, it was in the limits $40 \geqslant d \geqslant 16$ μm, depending on the plasma density. For comparison with Fig. 5 of Ref. [13], Fig. 3 shows our theoretical dependences on the plasma length $L$ for the 32.8-nm XRL quantum yield $N_{out}^{ph}(L)$. For the known density and geometry of the plasma we fitted $T_e$ so as to best reproduce the experimental dependence of the quantum yield on $L$. The $T_e$ value determined in this way is equal to 90 eV, which corresponds to an increase in quantum yield by ~2.5 orders of magnitude over a length from 3 to 4.5 mm. For $L \sim 4$ mm, the experimental curve flattens (see Fig. 5 in Ref. [13]), while our model curve in Fig. 3 is still far from saturation. This comparison suggests that the pump energy in the experiment was sufficient to pump the plasma of length of only $L \sim 4$ mm. This assumption was also made in Ref. [13] in the discussion of the experiment. We note that another, weaker laser line with $\lambda \approx 33.5$ nm was observed in Ref. [13] (see Fig. 1 of the present work as well as Fig. 2 in Ref. [13]).

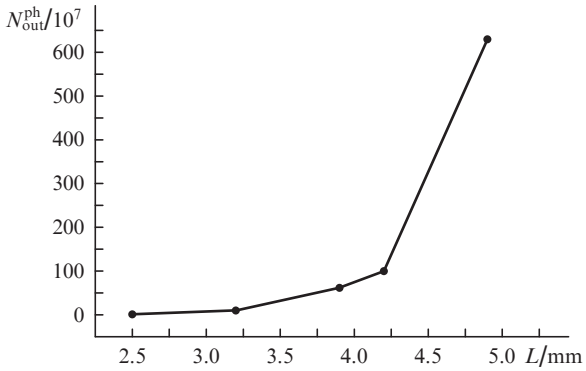


**Figure 3.** Calculated dependence of the quantum yield $N_{out}^{ph}$ on the plasma length $L$ for the 32.8-nm $Kr^{8+}$ XRL.

For comparison with the experimental dependence of the quantum yield $N_{out}^{ph}$ on the atomic krypton number density $n_{Kr}$ (for given $T_e$ and $L$) shown in Fig. 3 in Ref. [13], we performed calculations for $T_e = 90$ eV and $L = 4.5$ mm. The calculated dependence is shown in Fig. 4, where its highest value is normalised to unity. It is significant that $N_{out}^{ph}(n_{Kr})$ reaches its maximum value for a krypton pressure $p_{Kr} = 20$ Torr when $T_e = 90$ eV; for other $T_e$ values the peak of $N_{out}^{ph}(n_{Kr})$ shifts. A good agreement of our theoretical curve in Fig. 4 with the experimental one (see Fig. 3 in Ref. [13]) is achieved on taking into account a smooth decrease in the diameter of the active medium from 40 to 16 μm when $p_{Kr}$ is varied from 5 to 20 Torr. For $p_{Kr} \geqslant 20$ Torr the diameter $d \approx 16$ μm. Therefore, the value $T_e = 90$ eV was obtained in the analysis of two independent experiments of Ref. [13]. A 200-fold increase in $N_{out}^{ph}$ in the 3–4 mm interval corresponds to an average gain $G_{av} \sim 24$ cm$^{-1}$. The temporal $g(t)$ evolution calculated with the use of our model is shown in Fig. 5.

A similar dependence $N_{out}^{ph}(n_{Xe})$ obtained in an experiment on Xe [14] is shown in Fig. 3 in Ref. [13]. The experiment of Ref. [14] was performed for a significantly lower pump intensity $I_{pump} = 3\times10^{16}$ W cm$^{-2}$, but the maximum quantum yield of photons was two-three times higher than in Ref. [13], and we estimated $T_e$ at 140 eV. The higher temperature has the effect that the quantum yield in Ref. [14] is higher. For xenon the maximum quantum yield was observed for a gas pressure

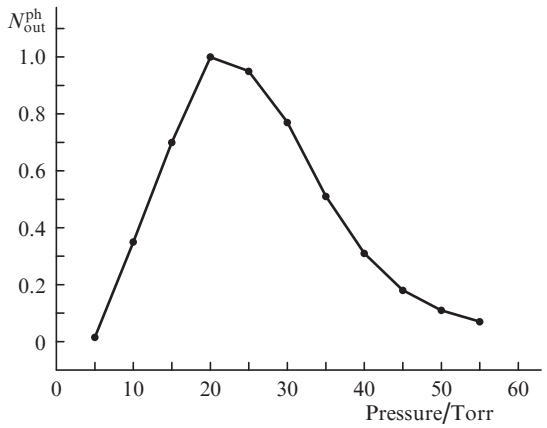


**Figure 4.** Calculated pressure dependence of the normalised quantum yield $N_{out}^{ph}$ for the 32.8-nm $Kr^{8+}$ XRL.

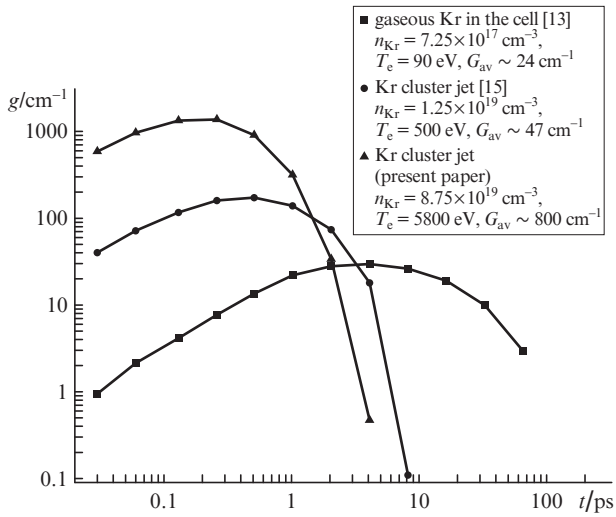


**Figure 5.** Time evolution of the gains calculated for a krypton XRL under different conditions.

of 15 Torr [14]. The nature of the extremum of the dependence of the XRL quantum yield on the gas pressure is easy to understand. Let us assume that $T_e$ is fixed; then the population inversion and $N_{out}^{ph}$ will increase with increasing pressure. However, with increasing pressure the 'mixing' of level populations will intensify due to electron–ion collisions, the plasma will tend to the equilibrium state, and the population inversion will decrease. Furthermore, with increasing pressure the rate of $Kr^{8+}$ ionisation to the states $Kr^{9+}$, $Kr^{10+}$, etc. will rise due to electron–ion collisions; in this case, the working ion density (the population inversion) will become smaller. The peak of the dependence of $N_{out}^{ph}$ on the plasma pressure corresponds to the balance of these processes. On further increasing the pressure, collisional level mixing and $Kr^{8+}$ ionisation prevail; in this case, the population inversion and $N_{out}^{ph}$ become smaller. The peak of $N_{out}^{ph}(p_{Kr})$ for $Kr^{8+}$ is located at a higher pressure than for $Xe^{8+}$ because the population mixing rates for $Kr^{8+}$ are approximately two times lower than for $Xe^{8+}$.

We note that recording the $Xe^{8+}$ laser line [14] is possible for the shortest length $L = 1.5$ mm, while the $Kr^{8+}$ laser line is observable only for $L = 3$ mm. This is attributable to the fact that the $Kr^{8+}$ laser line is enveloped by the background plasma emission for $L < 3$ mm.

The weak amplification of the laser line in the $Kr^{8+}$ plasma strongly suggests that the $T_e$ value obtained by way of OFI of krypton atoms is substantially lower than the theoretically predicted value [4]. According to the calculations performed in Refs [2, 13], from formula (3) of Ref. [4] it follows that the average energy of the eight electrons detached from a Kr atom upon its interaction with circularly polarised light should be equal to ~600 eV, which is at strong variance with the experimentally obtained value (90 eV) [13]. From the interpretation of the experimental results of Refs [13, 14] it follows that atomic electrons with a higher ionisation potential require a higher optical field intensity and possess a lower kinetic energy upon detachment. The former statement is obvious, the latter contradicts the conclusions of Refs [2, 13, 14] drawn from the classical principles of Ref. [4]. We believe that the one-electron approximation for calculating the energy of interaction between the outer atomic shell of noble elements and the electromagnetic field is true only for the OFI of the first electron, because its first excited state is sufficiently high. The energy of interaction between other outer-shell electrons and the electromagnetic field cannot be taken into account in the framework of the classical one-electron approximation, because it calls for the inclusion of a rather dense spectrum of strongly correlated states.

## 4. Preliminary experiments on the observation of 32.8-nm X-ray lasing in a krypton cluster jet

The first experiment on the observation of X-ray lasing in $Kr^{8+}$ in the interaction of a krypton cluster jet with the pump radiation was performed in Ref. [15]. In this work, use was made of a Ti:sapphire laser with a peak output power of 10 TW (45 fs, 235 mJ, 810 nm, 10 Hz) focused to a spot of diameter $d = 10$ μm, which corresponded to an intensity of $4\times10^{18}$ W cm$^{-2}$. The pump pulse was circularly polarised, the polarisation ellipticity was varied with a motorised $\lambda/4$ plate. The cluster jet was formed using a valve with a slotted nozzle; the target (plasma) length was equal to 9 mm. The pump pulse propagated along the slot. The experiment was executed in two versions: plasma production by one pump pulse or plasma irradiation by an 'ignition pulse' (45 fs, p-polarisation, 45 mJ) 2.5 ns after the pump pulse and by a 'plasma heating pulse' (45 fs, s-polarisation, 300 mJ) 80 ps later. The latter two pulses produced a so-called waveguide – a quasi-uniform plasma in the active state, which provided the propagation of an XRL pulse with a low angular divergence. All pump beams passed through an axicon.

Without the use of this waveguide, the maximum quantum yield $N_{out}^{ph} = 1.5\times10^8$ photons per pulse for $n_{Kr} = 6\times10^{17}$ cm$^{-3}$; the output XRL beam divergence was equal to 15 mrad. With the use of the waveguide, $N_{out}^{ph} = 8\times10^{10}$ photons per pulse for $n_{Kr} = 1.6\times10^{19}$ cm$^{-3}$, which corresponded to a conversion efficiency of $2\times10^{-6}$; the beam divergence was equal to 5.6 mrad. From Fig. 3 of Ref. [15] it follows that a high XRL yield is also possible for $n_{Kr} > 2\times10^{19}$ cm$^{-3}$ for the $T_e$ value achieved in that work. We note that in this experiment the plasma contained $Kr^{9+}$ and $Kr^{10+}$ ions upon irradiation by the first pump pulse of too high an intensity. Subsequently, for 2.5 ns the plasma recombined, expanded, and cooled down due to radiative loss to reach a state dominated by $Kr^{8+}$ ions; as this took place, the plasma became more uniform in the working region. Without the use of secondary (heating) pulses, the amplification proceeded in a cooling mode, at low $T_e$. The corresponding dependence of

$N_{out}^{ph}$ on $n_{Kr}$ is shown by empty circles in Fig. 3 of Ref. [15]. When use was made of the secondary pump pulses the plasma, which had recombined to the state where ground-state $Kr^{8+}$ ions prevailed, was heated again due to the inverse bremsstrahlung. It is evident that $T_e$ was substantially higher in the latter case, and the optimal value of $n_{Kr}$ increased to $\sim 2\times 10^{19}$ cm$^{-3}$. Shown in Fig. 5 of our work is the $g(t)$ dependence calculated for the plasma parameters borrowed from Ref. [15].

In the subsequent paper, Ref. [16], the experimental method for observing XRL radiation from the krypton cluster plasma was improved by using a high-order harmonic (25th) (HOH) of Ti:sapphire laser radiation, which was generated in gaseous argon and had the same wavelength as the XRL radiation. This HOH is also amplified when passing through the active medium. Amplified in the XRL is the superposed radiation of two waves, which affect each other. One of them (the HOH) has a high degree of coherence and an ultrashort duration. The effect of the HOH on the XRL line is rather strong. It shortens the XRL pulse duration and lowers the divergence of the amplified radiation as well as improves its coherence.

The output XRL radiation coherence was measured with a two-slit Young interferometer in Ref. [16]. When use was made of the HOH, the spatial coherence of the XRL radiation was found to be approximately four times higher in comparison with that measured when the HOH was not used. In Ref. [16], the quantum yield $N_{out}^{ph} = 10^{11}$ photons per pulse and the half-height XRL beam divergence was equal to 1.1 mrad. In a recent work by Chen et al. [1], use was made of the same XRL scheme as in Refs [15, 16], but the energy of the main pump pulse in Ref. [1] was equal to ~1 J. In Ref. [1] it was determined that a pump intensity of $\sim 2\times 10^{17}$ W cm$^{-2}$, when interacting with a jet of krypton clusters of size ~500 Å (more than $10^4$ atoms per cluster), gave rise to a plasma dominated by ions in the $Kr^{8+}$ charge state.

## 5. Model calculations of the radiation parameters of 32.8-nm XRL in a krypton cluster plasma

Experiments with cluster plasmas [1, 15, 16] were intended to accomplish the task of achieving a high degree of coherence in a relatively long plasma with $L \sim 1$ cm. In this case, the plasma with a temperature of ~10 keV cooled down during its recombination time (2.5 ns) to reach a state dominated by the working ion $Kr^{8+}$. Therefore, almost all of the deposited energy was radiated during the recombination time. Our main idea is that a high conversion coefficient and a high degree of coherence may be obtained in an extremely small plasma volume $V \sim 10^{-8}$ cm$^3$ due to the use of extremely high values of $T_e$ and $n_{Kr}$. We list the main prerequisites to the development of high-efficiency XRLs in cluster jets:

1. Absorption of more than 90% of the pump energy; this was implemented, for instance, in the experiment of Ref. [17] for rare-gas cluster jets for a peak plasma pump intensity of $\sim 10^{17}$ W cm$^{-2}$.

2. Weak reflection of the pump beam from the cluster jet and the absence of plasma debris.

3. Attainment of electron energies of several kiloelectron volts. In particular, Shao et al. [18] recorded an energy distribution of electrons with energies of several kiloelectron volts, which was produced by high-intensity laser irradiation of a xenon cluster jet. In earlier experiments [19] it was determined that high electron temperatures are achieved upon irradiation of sufficiently large krypton and xenon clusters: for a cluster diameter of 150 Å, temperatures $T_e > 1$ keV are achieved for an intensity of $\sim 10^{16}$ W cm$^{-2}$, and raising the intensity up to $5\times 10^{16}$ W cm$^{-2}$ gives Te~10 keV (see Fig. 9 in Ref. [19]).

4. Control over the plasma density and temperature as well as ionisation balance.

5. For a high velocity of the cluster jet the XRL may operate with a repetition rate of ~125 kHz [20].

The large number of parameters characterising a) the plasma and its parameters, b) the nozzle, the pressure in the gas reservoir and the cluster size, and c) the laser pump pulse should be matched to each other using a theoretical model. Then, the active medium, in principle, may be produced by a single main pump pulse. This is possible when the model provides an adequate reproduction of experimental data.

The cluster size is critically important for the high-temperature plasma production in the interaction of an ultrashort pump pulse with the cluster jet. The pulse pedestal is usually several nanoseconds long; in the course of pedestal–cluster interaction, there occurs cluster heating, electron escape from its surface, and its expansion. The highest $T_e$ value is reached when the electron density $n_e$ of the cluster nanoplasma is equal to $3n_{crit}$ ($n_{crit} = \pi c^2 m_e/(e^2\lambda^2)$); in this case, there occurs a resonance input of laser radiation energy to the plasma energy [19]. To maximise the energy input, the pedestal duration and intensity should correspond to the cluster size: when the cluster is too small (it rapidly expands to reach $3n_{crit}$), the cluster disintegration proceeds too fast (prior to the arrival of the main high-intensity pulse), and $T_e$ is not high. When the cluster is too large (its expansion takes too long), the cluster disintegration takes place after the passage of the high-intensity pulse and $T_e$ is not high, either. For a cluster of correct size, $n_e = 3n_{crit}$ at the instant of arrival of the main femtosecond pump pulse: in this case, the plasma temperature $T_e$ assumes the highest possible value.

The variation of the cluster size in relation to the pressure and temperature of gas in the stagnation chamber as well as to the valve geometry has been adequately studied for cone-shaped nozzles with a round orifice, for which the number of atoms in rare-gas clusters is usually determined by Rayleigh scattering with the use of an empirical formula from Ref. [21]. Recently a start was made on the investigation of the cluster size in relation to the gas pressure in the stagnation chamber in the case of a slotted nozzle. In particular, a slotted supersonic nozzle was shown to provide a significantly higher number of atoms in a cluster in comparison with a cone-shaped nozzle [22].

The dependence of plasma electron and ion energies on the cluster size was studied in many papers, for instance in Refs [18, 23]. In Ref. [18] the xenon cluster jet was exposed to laser radiation with a peak intensity of $10^{16}$ W cm$^{-2}$; the clusterisation of xenon atoms was shown to set in upon raising the pressure in the stagnation chamber up to ~1 bar. With increasing pressure the cluster size became larger, resulting in a sharp rise in the electron temperature in the plasma (see Fig. 2 in Ref. [18]). The density dependence of $T_e$ is in qualitative agreement with our result reported in Ref. [7] and shown there in Fig. 4. To extend this dependence to the domain of higher plasma density ($n_i \geqslant 10^{18}$ cm$^{-3}$, which corresponds to a cluster size of no less than $10^3$ atoms per cluster) we take advantage of Fig. 4 from Ref. [23]. The resultant dependence of $T_e$ on $n_{Kr}$ is given in Fig. 6. The inset in Fig. 6 shows the dependence of $T_e$ on the cluster size for Xe and Kr. These dependences will be used in our calculations of the gain $g(t)$.

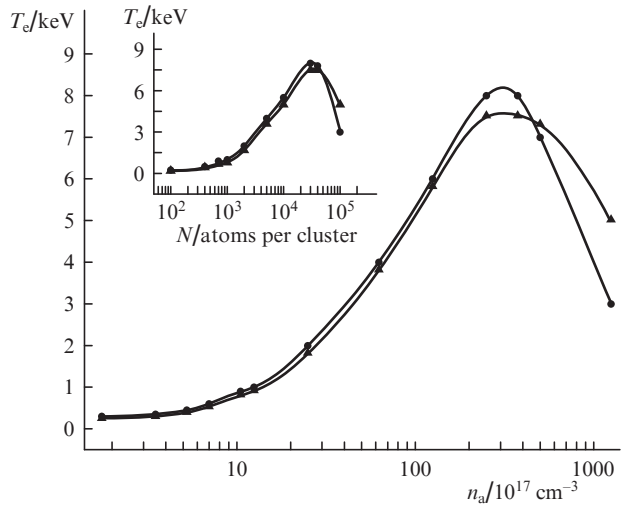


**Figure 6.** Dependences of the electron temperature $T_e$ in Xe (●) and Kr (▲) plasmas on the atomic number density $n_a$ obtained using our calculations [7] as well as the experimental and theoretical data of Ref. [23]. The inset shows the dependences of the plasma electron temperatures on the number $N$ of atoms in the clusters.

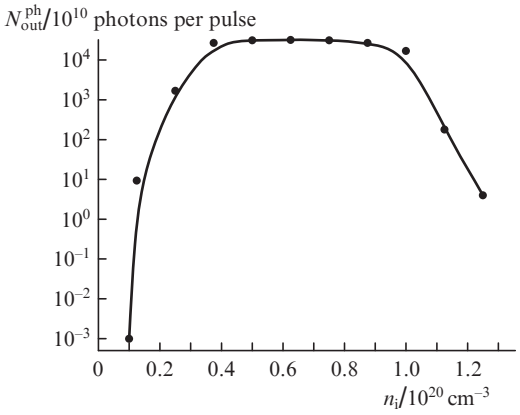


**Figure 7.** Quantum yield of 32.8-nm XRL with a pulse duration of ~1 ps and a volume of ~$10^{-8}$ cm$^3$ calculated as a function of $Kr^{8+}$ ion density for $T_e$ = 5800 eV.

One can see from Fig. 6 that the lowering of $T_e$ for Kr clusters takes place for larger cluster sizes (higher atomic densities $n_a$). This signifies that in the high-density domain it is possible to make a higher-efficiency XRL in $Kr^{8+}$ than in $Xe^{8+}$.

The XRL calculation model was used in our previous works [6–8], which cite references to the papers describing the theoretical approach in detail. A brief statement of the theoretical approach is given in Section 2. When a cluster jet is used as a target, the plasma heating results from the explosion of a weakly ionised expanding cluster; after the explosion, initially $T_i \gg T_e$, but the electron–ion temperature equalising occurs in a time $t \leqslant 100$ fs for a high plasma density ($n_i \geqslant 10^{19}$ cm$^{-3}$). That is why in our calculations we assume that $T_e = T_i$, which has a pronounced effect on the Doppler contribution to the laser transition linewidth. For high densities ($n_i \geqslant 10^{19}$ cm$^{-3}$) the line broadening caused by electron–ion collisions nevertheless exceeds the Doppler broadening.

We determine the optimal plasma parameters using the dependences of $T_e$ and $T_i$ on the atomic density $n_{Kr}$ (Fig. 6). The temporal evolution $g(t)$ for the optimal parameters $n_{Kr} = 8.75\times10^{19}$ cm$^{-3}$, $T_e$ = 5800 eV, and $d$ = 12 μm is shown in Fig. 5. The peak $g(t)$ value exceeds 1000 cm$^{-1}$. The gain averaged over a time $t$ = 1 ps is $G_{av} \approx 800$ cm$^{-1}$. Shown for comparison in Fig. 5 are the dependences $g(t)$ and the $G_{av}$ values for an XRL produced by the OFI of gaseous krypton [13], where the averaging is performed over a time $t \approx 20$ ps. Also shown in Fig. 5 is the evolution $g(t)$ in cluster plasma [15] heated by secondary pump pulses on cooling (the averaging is performed over a time $t \approx 10$ ps). We note that $t$ = 10 ps corresponds to the spatial scale length of XRL pulses of the order of 3 mm. The propagation of a pulse with this spatial scale length was observed in Ref. [24], in which experimental conditions were the same as in Ref. [15].

We calculate the quantum yield for a cylinder with $L$ = 300 μm, $d$ = 12 μm (of volume $V = 3.4\times10^{-8}$ cm$^3$) over a period $t$ = 1 ps; its density dependence is shown in Fig. 7. One can see that $N_{out}^{ph} > 10^{14}$ photons per pulse in broad density range: $n_i \approx (4–9)\times10^{19}$ cm$^{-3}$. This corresponds to $n_e \approx (3–8)\times10^{20}$ cm$^{-3}$. Under the assumption that $n_i = 4\times10^{19}$ cm$^{-3}$, $n_e = 3\times10^{20}$ cm$^{-3}$, the absorbed pump energy in the volume $V$ should be equal to $\sim8\times10^{16}$ eV.

## 6. Experimental facility

It is well known [22] that the pressure dependence of the average cluster size is strongest for a slotted valve. The use of a supersonic nozzle to produce large clusters is more efficient than the use of a sonic one. We employ a slotted supersonic nozzle with a slot width of 500 μm and an opening angle of 24°. The krypton pressure above the valve is varied in the 35–45 atm range. The valve operates in a pulsed regime. At least two cone-shaped diaphragms with slots (skimmers) are placed in the path of the cluster jet. The diaphragms form a cluster beam of prescribed density; its cross section is a 5-mm long rectangle of width 300 μm. The width of the cluster beam defines the plasma filament length $L$. The pump and HOH pulses are focused into the cluster jet perpendicular to the axis of the slotted nozzle. For the indicated pressures the gas phase is practically missing from the cluster jet.

The optical setup of the experimental facility for generating an ultrashort XRL pulse from $Kr^{8+}$ ions is schematised in Fig. 8. The krypton cluster jet (*1*) is rectangular in shape and is directed perpendicular to the plane of Fig. 8, so that the focused pump laser radiation touches the lower edge of the rectangular cross section of the krypton cluster jet. This is done to minimise the loss of cluster plasma radiation due to its absorption in the direction perpendicular to the optical axis (*2*) of the XRL. To pump the plasma and make femtosecond gates, use is made of a Ti:sapphire laser system (810 nm), which generates four independent laser pulses: the main (*3*) and three auxiliary pulses (*4*, *5*, and *6*) delayed relative to the main one. The main pulse with an intensity of ~$10^{17}$ W cm$^{-2}$ ionises krypton clusters to produce the plasma dominated by $Kr^{8+}$ ions. The first auxiliary laser pulse (*4*) with an energy of ~1 mJ interacts with gaseous argon to generate the 25th harmonic (HOH), which enters the cluster plasma (*1*) with a delay of ~100 fs relative to the main pump pulse (*3*). The HOH radiation decreases the XRL beam divergence and its pulse duration as well as improves the spatial beam coherence. The second (*5*) and third (*6*) auxiliary pulses produce ultrafast plasma gates, which are employed in the recording of plasma parameters and XRL radiation.

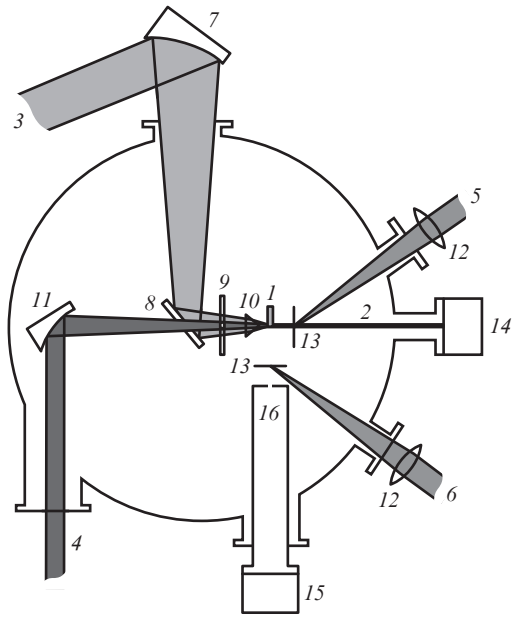


**Figure 8.** Schematic representation of the facility for obtaining an ultrashort XRL pulse:
(*1*) krypton cluster jet; (*2*) XRL axis; (*3*) main pump pulse; (*4*) HOH pulse after the first delay line; (*5*) and (*6*) pulses after the second and third delay lines (ultrafast optical plasma gates); (*7*) off-axis parabolic mirror; (*8*) plane deflecting mirror; (*9*) polariser; (*10*) axicon; (*11*) multilayer parabolic mirror; (*12*) lenses; (*13*) aluminium filters; (*14*) grazing-incidence spectrometer with a CCD camera; (*15*) pinhole camera; (*16*) high vacuum region of the measuring channel.

The energy of the main laser pulse is equal to 10 mJ and its duration to 50 fs; the contrast ratio is higher than $10^7$ for $t \sim$ 10 ns, higher than $10^6$ for $t \sim 50$ ps, and higher than $10^4$ for $t \sim 1$ ps. The diameter of the laser focal spot on the surface of the cluster jet is equal to 10 μm.

The exact XRL–HOH wavelength match is achieved using chirp tuning in the HOH generation. The argon cell length is optimised at 6.5 mm, and the argon pressure is equal to ~22 Torr. The main laser beam is focused into the krypton cluster jet using an off-axis parabolic mirror (*7*), after which the pulse is reflected from a plane deflecting mirror (*8*), passes through a polariser (*9*), and forms with the help of an axicon (*10*) an extended caustic with a Besselian intensity distribution over cross section of the cluster jet.

With the use of a multilayer parabolic mirror (*11*) ($\lambda$ = 32.8 nm), the HOH pulse is also focused, coaxially with the main pulse, into the krypton cluster jet after passing through a polariser (*9*) and the central openings in the mirror (*8*) and the axicon (*10*). The ellipticity of the polarisation of both pulses is optimised with the polariser (*9*).The HOH pulse enters the cluster plasma ~100 fs after the termination of the main pump pulse. The auxiliary pulses (*5*) and (*6*) pass respectively through the second and third delay lines to produce ultrafast gates, which absorb the residual radiation in a time $t \leqslant 1$ ps after the onset of X-ray lasing. Lenses (*12*) focus the pulses (*5*) and (*6*) onto aluminium foils of thickness 300–400 nm, which are usually employed as filters when recording 30–40-nm radiation. These laser pulses provide the ultrafast ionisation (explosion) of the outer part of the foil filters and transforms them to a low-temperature plasma, which absorbs the afterglow of the active plasma region. In the course of alignment and synchronisation of the facility, the filters were mechanically changed prior to every laser pulse in order to ensure reproducibility of the conditions of foil plasma production.

Two channels are used to diagnose the plasma parameters and XRL radiation: in one channel the parameters are recorded along the optical XRL axis (*14*) and in the other channel they are recorded perpendicular to the axis (*15*). In this case, in order that the XRL spectrum does not broaden in channel (*15*), the measuring channel (*16*) is made as close as possible to the cluster plasma and evacuated to a pressure of $10^{-8}$ Torr (for a background krypton pressure in the vacuum chamber of $10^{-5}$ Torr). An aluminium filter separates the high-vacuum zone from the low-vacuum one. Diagnostic instruments may be attached to the flanges of the measuring channels in different combinations.

The XRL and HOH wavelengths are recorded using a grazing-incidence spectrometer with a CCD camera. An interferometric technique is used to measure the line profile. This is due to the fact that, owing to the high amplification coefficients, the spectra of output XRL and HOH radiation pulses will be extremely narrow lines of width ~1 mÅ, whose profiles cannot be resolved with a diffraction spectrometer. The absolute output energy and therefore the XRL efficiency are measured with an absolute-calibrated photodiode AXUV-100G (IRD, Inc.) (*14*) located in the XRL axis. To this end, the fraction of radiated energy transmitted through the aluminium filter is calculated, and account is taken of the photodiode sensitivity and the filter transmission. To record the spatial characteristics of the radiating plasma, use is made of the pinhole camera and the CCD camera. The evolution of the amplified pulse propagation along the plasma filament is recorded in the transverse direction. The instant this camera begins to record the spectrum is timed to the instant of arrival of the main pump pulse to the cluster jet. The CCD camera located in the axis of the plasma filament measures the XRL divergence. It is planned to perform the first experiments without using the HOH and the axicon in order to optimise the polarisation ellipticity and the cluster parameters in the jet.

## 7. Conclusions

According to our comprehensive calculations, the scheme for $Kr^{8+}$ is highest in efficiency among the three similar OFI-based XRL schemes outlined in Ref. [2] and shown in Fig. 1. The generation of radiation of a high-efficiency XRL with an ultrashort active region produced in a krypton cluster jet relies on the possibility of achieving a temperature $T_e \geqslant 5$ keV for a density $n_{Kr}^{opt} = (4–8)\times10^{19}$ cm$^{-3}$, which turns out to be optimal. We note that $n_{Xe}^{opt}$ is significantly lower when we are dealing with the production of a cluster plasma XRL on the $\lambda$ = 41.8 nm transition in $Xe^{8+}$ [7], where the pulse duration $t \sim$ 5 ps and $L \geqslant 1.5$ mm under optimal conditions. The high $Kr^{8+}$ XRL efficiency calls for the fulfilment of three fundamental requirements:

1. Fast excitation of the upper working level $3d^94d\,^1S_0$ ($J = 0$) from the ground state $3d^{10}$.

2. Fast ionisation of $Kr^{8+}$ to the higher ionisation stages $Kr^{9+}$ and $Kr^{10+}$ due to electron–ion collisions.

3. A high value of the gain $G_{av}$ averaged over a period $t = 1$ ps.

We point out that it is possible to achieve an approximately hundred times higher quantum yield from a subpicosecond $Kr^{8+}$ XRL than from a $Xe^{8+}$ XRL [8]. This is because

in the case of krypton it is possible to advance to the domain with a higher density $n_{Kr}$ in the production of a high-temperature plasma with $T_e \sim 5000$ eV (see Fig. 6). Furthermore, the level mixing due to electron–ion collisions (transition to the equilibrium state) in $Kr^{8+}$ proceeds approximately two times slower than in $Xe^{8+}$. It is also significant that the ionisation of $Kr^{8+}$ on a picosecond time scale proceeds in a higher-density plasma than the $Xe^{8+}$.

The ionisation balance is controlled by varying the intensity of pump laser radiation; in particular, an intensity of $\sim(1-2)\times10^{17}$ W cm$^{-2}$ is sufficient for obtaining a plasma dominated by $Kr^{8+}$ ions. The radiation of ordinary femtosecond lasers has a prepulse several nanoseconds in duration, which determines the cluster size for achieving the maximum energy input from the main femtosecond pump pulse.

The feasibility of making a $Kr^{8+}$ XRL with a total pump energy conversion coefficient of $5\times10^{-3}$ is indirectly borne out by recent experiments [1, 24], where a relatively high ($5\times10^{-6}$) $Kr^{8+}$ XRL conversion coefficient was observed in a plasma filament of length $L \sim 0.9$ cm, diameter $d = 12$ μm, and density $n_{Kr} \sim 1.6\times10^{19}$ cm$^{-3}$ for $I_{pump} \sim 4\times10^{18}$ W cm$^{-2}$. For so high an intensity, the plasma was initially dominated by higher-ionised ions than $Kr^{8+}$. Initially $T_e$ was equal to ~10 keV; it is easy to estimate that 2.5 ns later, upon recombination and radiation, so high a density plasma lost almost all energy deposited into it. Our model suggests that this energy should be used for X-ray lasing due to increasing the ion density and obtaining giant $G_{av}$ values for a submillimetre length of the plasma filament.

From the experiments of Refs [15, 16] it follows that the cluster jet plasma is produced immediately after the action of a pump pulse. The $\lambda = 32.8$ nm radiation is negligible during the cluster expansion. At a high plasma density the intensity of X-ray lasing reaches its maximum in 100 fs (see Fig. 5). Therefore, in the XRL project under consideration it is possible to obtain an output pedestal-free pulse with an extremely steep leading edge; the output pulse is also characterised by a steep trailing edge. This pulse shape shows good promise for studying ultrafast processes.

***Acknowledgements.*** The authors express their appreciation to G.N. Makarov and S.V. Chekalin for their interest in the work and helpful discussions.

## References

1. Chen B.K. et al. *Appl. Phys. B*, **106**, 817 (2012).
2. Lemoff B.E., Barty C.P.J., Harris S.E. *Opt. Lett.*, **19**, 569 (1994).
3. Ivanov L.N., Ivanova E.P., Knight L.V. *Phys. Lett. A*, **206**, 89 (1995).
4. Corkum P.B., Burnett N.H., Brunel F. *Phys. Rev. Lett.*, **62**, 1259 (1989).
5. Rocca J.J., Clark D.P., Chilla J.L.A., Slyaptsev V.N. *Phys. Rev. Lett.*, **77**, 1476 (1996).
6. Ivanova E.P., Zinov'ev N.A. *Kvantovaya Elektron.*, **27**, 207 (1999) [*Quantum Electron.*, **29**, 484 (1999)].
7. Ivanova E.P. *Phys. Rev. A*, **84**, 3829 (2011).
8. Ivanova E.P. *Kvantovaya Elektron.*, **42**, 1100 (2012) [*Quantum Electron.*, **42**, 1100 (2012)].
9. Larroche O., Ros D., Klisnick A., Sureau A., Möller C., Guennou H. *Phys. Rev. A*, **62**, 043815 (2000).
10. Kim C.M., Janulewicz A., Kim H.T., Lee J. *Phys. Rev. A*, **80**, 053811 (2009).
11. Zhang J. et al. *Science*, **276**, 1097 (1997).
12. Ivanova E.P., Zinoviev N.A. *J. Phys. IV. France*, **11**, Pr2-151 (2001).
13. Sebban S. et al. *Phys. Rev. Lett.*, **89**, 253901 (2002).
14. Sebban S. et al. *Phys. Rev. Lett.*, **86**, 3004 (2001).
15. Chou M.-C. et al. *Phys. Rev. Let.*, **99**, 063904 (2007).
16. Lin P.H. et al. *Opt. Lett.*, **34**, 3562 (2009).
17. Ditmire T., Smith R.A., Marjoribanks R.S., Kulcsar G., Hutchinson M.H.R. *Appl. Phys. Lett.*, **71**, 166 (1997).
18. Shao Y.L., Ditmire T., Tisch J.W.G., Springate E., Marangos J.P., Hutchinson M.H.R. *Phys. Rev. Lett.*, **77**, 3343 (1996).
19. Ditmire T., Donelly T., Rubenchik A.M., Falcone R.W., Perry M.D. *Phys. Rev. A*, **53**, 3379 (1996).
20. Ter-Avetisyan S., Vogt U., Stiel H., Schnürer M., Will I., Nickles P.V. *J. Appl. Phys.*, **94**, 5489 (2003).
21. Hagena O.F., Obert W. *J. Chem. Phys.*, **56**, 1793 (1972).
22. Chen G., Kim B., Ahn B., Kim D.E. *J. Appl. Phys.*, **106**, 053507 (2009).
23. Springate E., Hay N., Tisch J.W.G., Mason M.B., Ditmire T., Hutchinson M.H.R., Marangos J.P. *Phys. Rev. A*, **61**, 063201 (2000).
24. Chou M.-C., Lin P.-H., Hung T.-S., Lin J.-Y., Wang J., Chen S.-Y. *Phys. Rev. A*, **74**, 023804 (2006).